Vol 13 No 8, August 2004
1009-1963/2004/13(08)/1191-10
Chinese Physics

Vertically forced surface wave in weakly viscous fluids bounded in a circular cylindrical vessel*

Jian Yong-Jun(菅永军)[a)b)†] and E Xue-Quan(鄂学全)[b)]

[a)] *First Institute of Oceanography, State Oceanic Administration, Qingdao* 266061, *China*

[b)] *Institute of Mechanics, Chinese Academy of Sciences, Beijing* 100080, *China*

(Received 27 November 2003; revised manuscript received 24 March 2004)

Two-time scale perturbation expansions were developed in weakly viscous fluids to investigate surface wave motions by linearizing the Navier–Stokes equation in a circular cylindrical vessel which is subject to a vertical oscillation. The fluid field was divided into an outer potential flow region and an inner boundary layer region. A linear amplitude equation of slowly varying complex amplitude, which incorporates a damping term and external excitation, was derived for the weakly viscid fluids. The condition for the appearance of stable surface waves was obtained and the critical curve was determined. In addition, an analytical expression for the damping coefficient was determined and the relationship between damping and other related parameters (such as viscosity, forced amplitude, forced frequency and the depth of fluid, etc.) was presented. Finally, the influence both of the surface tension and the weak viscosity on the mode formation was described by comparing theoretical and experimental results. The results show that when the forcing frequency is low, the viscosity of the fluid is prominent for the mode selection. However, when the forcing frequency is high, the surface tension of the fluid is prominent.

Keywords: vertically forced oscillation, weakly viscid fluid, surface wave modes, singular perturbation expansions, damping coefficient

PACC: 0340G, 4754, 5235M, 9530L

1. Introduction

The study of surface waves on a fluid via vertical vibration in a closed cylindrical vessel has a long history. The earliest experiment to describe these phenomena dates back to Faraday.[1] He put a vessel filled with different fluids on a vertically vibrating plate, and the free surface of the fluid formed various beautiful surface waves. He realized that these surface waves have a frequency equal to one-half that of the excitation and belong to subharmonic resonance. Benjamin and Ursell[2] were the first to consider the linear stability analysis for ideal liquids of the plane surface. They showed that the linear dynamics of the amplitudes of the surface modes is governed by Mathieu's equation, which allows for harmonics as well as subharmonics. Miles[3−5] has studied nonlinear effects, adopting a variational approach. A review of this subject is given by Miles and Henderson.[6] Faraday resonance has proven to be an ideal (experimental, computational, and analytical) laboratory to study nonlinear systems, bifurcation, and pattern formation, creating a wealth of studies.

Recent experiments with viscous liquids show stripes,[7] a regular triangular pattern,[8] and competing hexagons and equilateral triangles[9] at the free surface, in contrast to the earlier experiments with low viscosity fluids (see, for instance, Refs.[10–12]), showing square patterns at the onset. These experimental observations suggested the importance of viscosity in pattern formation under parametric excitation.

E and Gao[13−15] carried out the flow visualization on surface wave patterns in a circular cylindrical vessel subjected to vertical external vibrations. They obtained very beautiful photographs of free surface patterns in wider driven frequencies, and most of them have not been reported before.

Recently, an approximate theoretical treatment associated with the experiments of E[13−15] was proposed by Jian and E,[16,17] from which the second-

*Project supported by the National Natural Science Foundation of China (Grant Nos 19772063, 19772068).
†Corresponding author. E-mail: jianyongjun@yahoo.com.cn

order free surface displacements and their contours were obtained by the two-time scale singular perturbation expansion in ideal fluids. In the following, the influence of surface tension was considered by Jian[18] and the theoretical result is much closer to the experimental results than that without surface tension. Although in the numerical results the contours of free surface waves agreed well with the experimental visualization, the forced frequency showed large difference. The poor agreement between theory and experiment is not surprising, as so many physical processes were involved in experiments that it was impossible to sort them out.

Due to the viscid dissipation in actual physical modelling, the determination of the damping coefficient is an essential problem. Our purpose in this paper is to derive the damping coefficient analytically, which is often obtained empirically. Hill[19] studied the Faraday resonance of interfacial waves in a two-layer weakly viscous system in a rectangular domain. He applied a perturbation technique to determine an approximate expression for the damping coefficient analytically in the vicinity of the boundary layer. Following this method, in this paper, we divide the whole stream field into outer potential flow region and inner boundary layer region. Both of the solutions for these two domains are derived by the method of multiple-scale expansion. The damping coefficient is deduced analytically by solvability condition of higher-order solutions. Finally, the influence of both surface tension and the weak viscosity on the pattern formation is described by a comparison between theoretical and experimental results.

The nonlinear evolution equation (65) in Refs.[16,17] can be modified by introducing the above linear damping, and the stability of the modified amplitude equation can also be studied, which will be given in another paper.

2. Governing equation and their linearization in weakly viscous fluids

Now we consider the surface wave excited by vertical oscillation of a circular cylindrical basin filled with weakly viscous fluids. All parameters and the choice of the coordinate system in Fig.1 are the same as in Refs.[16] and [17].

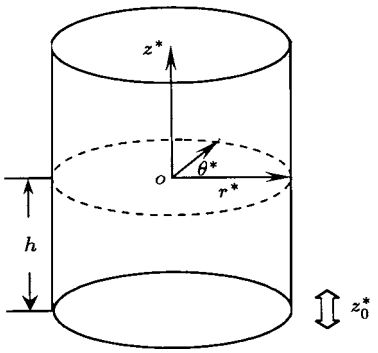

Fig.1. Physical model of the liquid-filled circular cylinder.

We suppose the fluid is incompressible, and $\boldsymbol{v}$ (r, θ, z, t) is the velocity field of the fluid, which obeys the Navier–Stokes equation

$$\frac{\partial \boldsymbol{v}}{\partial t} + \boldsymbol{v}\cdot\nabla\boldsymbol{v} = -\frac{1}{\rho}\nabla p - g(t)\boldsymbol{e}_z + \nu\nabla^2\boldsymbol{v}, \qquad (1)$$

where ρ is the mass density, p is the pressure, ν is the kinematic viscosity and $g(t)$ is the effective gravity acceleration, i.e. g minus the acceleration of the vibrating tank $\ddot{z}_0$,

$$g(t) = g - \ddot{z}_0 = g + 4A\omega_0^2\cos 2\omega_0 t. \qquad (2)$$

Let η (r, θ, t) be the displacement of the surface from z=0. In order to allow for a unique solution of the Navier–Stokes equation, one must specify the boundary conditions. The appropriate boundary conditions for the free surface at z=η (r, θ, t) are the kinematic condition

$$w(r,\theta,z,t)|_{z=\eta} = \frac{\partial\eta}{\partial t} + \boldsymbol{v}\cdot\nabla\eta, \qquad (3)$$

where $|_\eta$ means the evaluation at $z=\eta$, and w denotes the velocity in the z direction. At the liquid–air interface z=η (r, θ, t), the net force per unit area is balanced by the surface tension Γ, thus we have

$$(T_{jk}^{\mathrm{air}} - T_{jk})\cdot n_k = \Gamma\left(\frac{1}{R_1}+\frac{1}{R_2}\right)n_j. \qquad (4)$$

Here T_{jk}^{air} and T_{jk} denote the stress tensor of the air and liquid respectively, $\boldsymbol{n}$ is the unit outward normal to the surface, Γ the surface tension, and R_1 and R_2 are the radius of curvature of the surface calculated using the principal axes. Because the dynamic viscosity of air is smaller than that of a liquid, the stress tensor of the air above the liquid layer can be approximated by a constant atmospheric pressure. Thus we have

$$\begin{cases} T_{jk}^{\mathrm{air}} \approx -p_0\delta_{jk}, \\ T_{jk} = -p\delta_{jk} + \rho\nu\left(\dfrac{\partial v_k}{\partial x_j} + \dfrac{\partial v_j}{\partial x_k}\right), \end{cases} \qquad (5)$$

where p_0 is the atmospheric pressure which we assume to be constant, and δ_{jk} is the Kronecker δ operator. For the bottom and the side-wall we must use the non-slip condition as their boundary conditions

$$\boldsymbol{v}(r,\theta,z,t)=0. \tag{6}$$

For a sufficiently small drive amplitude A, the fluid remains at rest and the surface is flat. It is therefore convenient to introduce the pressure function Π $(r,\ \theta,\ z,t)$ from Eqs.(4) and (5), and we let

$$\Pi(r,\theta,z,t)=p(r,\theta,z,t)-p_0+\rho g(t)z, \tag{7}$$

so Eq.(1) is changed to

$$\frac{\partial \boldsymbol{v}}{\partial t}+\boldsymbol{v}\cdot\nabla\boldsymbol{v}=-\frac{1}{\rho}\nabla\Pi+\nu\nabla^2\boldsymbol{v}. \tag{8}$$

At the free surface, Eq.(4) can be divided into the normal part, which is perpendicular to the free surface

$$\begin{aligned}&\Pi(r,\theta,z,t)|_{z=\eta}-\rho g(t)\eta-2\rho\nu\frac{\partial w}{\partial z}\\ =&\Gamma\left(\frac{1}{R_1}+\frac{1}{R_2}\right),\end{aligned} \tag{9}$$

and the tangential part to the free surface

$$\rho\nu\left(\frac{\partial u}{\partial z}+\frac{\partial w}{\partial r}\right)=\rho\nu\left(\frac{1}{r}\frac{\partial w}{\partial\theta}+\frac{\partial v}{\partial z}\right)=0, \tag{10}$$

where u and v denote the velocity components in r and θ directions respectively.

The governing equation (8), boundary conditions of the free surface, i.e. Eqs.(3), (9), (10), and boundary condition for the side-wall and bottom, Eq.(6), describe the motion of the vertically excited surface wave in a viscous fluid.

In the case of ideal fluids, if we retain only the linear terms of Eq.(8), and suppose the wave motion is irrotational, we have

$$\Pi(r,\theta,z,t)=-\rho\frac{\partial\phi}{\partial t}, \tag{11}$$

where ϕ $(r,\ \theta,\ z,t)$ is the inviscid velocity potential. Now we take Eq.(11) as the approximate function when we consider the weakly viscous liquid as follows. As for the linear viscous problem, it is reasonable to separate the velocity into two components,

$$\boldsymbol{v}=\nabla\phi+\boldsymbol{U}, \tag{12}$$

namely, potential flow and boundary layer velocity. Here the velocity vector $\boldsymbol{U}$ is relevant to boundary layers while the potential part is important in the rest of the fluid. Substituting Eqs.(11) and (12) into Eq.(8), and ignoring the nonlinear terms, we obtain the following diffusive equation with respect to the velocity of boundary layer:

$$\frac{\partial\boldsymbol{U}}{\partial t}=\nu\nabla^2\boldsymbol{U}. \tag{13}$$

If we insert Eq.(12) into the incompressible condition $\nabla\cdot\boldsymbol{v}=0$, then the boundary layer velocity satisfies the zero divergence condition

$$\nabla\cdot\boldsymbol{U}=0. \tag{14}$$

Substituting Eq.(12) into Eqs.(3), (9), (10) and (6), and neglecting all nonlinear terms, the incompressible condition can be expressed as

$$\begin{aligned}&\frac{\partial^2\phi}{\partial r^2}+\frac{1}{r}\frac{\partial\phi}{\partial r}+\frac{1}{r^2}\frac{\partial^2\phi}{\partial\theta^2}+\frac{\partial^2\phi}{\partial z^2}=0,\\ &-h\le z\le\eta(r,\theta,t),\quad 0<r<R.\end{aligned} \tag{15}$$

The boundary conditions at the free surface

$$\frac{\partial\eta}{\partial t}-\frac{\partial\phi}{\partial z}=W,\quad z=\eta(r,\theta,t); \tag{16}$$

$$\begin{aligned}&\frac{\partial\phi}{\partial t}+g\left(1+\frac{4A\omega_0^2}{g}\cos 2\omega_0 t\right)\eta\\ &+2\nu\left(\frac{\partial^2\phi}{\partial z^2}+\frac{\partial W}{\partial z}\right)=0,\quad z=\eta(r,\theta,t);\end{aligned} \tag{17}$$

$$\rho\nu\left(\frac{\partial u}{\partial z}+\frac{\partial w}{\partial r}\right)=\rho\nu\left(\frac{1}{r}\frac{\partial w}{\partial\theta}+\frac{\partial v}{\partial z}\right)=0, \tag{18}$$

and the non-slip condition on the side-wall and at the bottom

$$\nabla\phi+\boldsymbol{U}=0,\quad z=-h\ \text{ and }\ r=R \tag{19}$$

must be satisfied. Here W is the component of boundary layer velocity $\boldsymbol{U}$ in the z direction. Equations (13)–(19) are elementary linearized equations in viscous fluids. Our aim is to study the weakly viscous surface waves via solving the above potential flow and boundary layer equations.

3. Nondimensional equations and establishment of curvilinear coordinates

Taking the radius R of the tank as the length scale, nondimensionalizing all related independent

variables and unknown variables, the following scalings are adopted:

$$\begin{aligned} z^* =& z/R, \quad r^* = r/R, \quad \eta^* = \eta/R, \\ t^* =& t/\sqrt{R/g}, \phi^* = \phi/(R\sqrt{gR}), \quad A^* = A/R, \\ \omega_0^* =& \omega_0/\sqrt{g/R}, \quad \varepsilon^* = 4A\omega_0^2/g, \\ \nu^* =& \nu/(\varepsilon^{*2}R\sqrt{gR}), \quad \boldsymbol{U}^* = \boldsymbol{U}/\sqrt{gR}, \end{aligned} \tag{20}$$

where the asterisks denote dimensionless quantities and they will be dropped subsequently. The parameter ε quantifies the acceleration due to the vertical oscillation relative to gravity and is assumed to be much less than unity.

We have supposed that the viscosity is weak, and has been scaled as ε^2 in Eq.(20) in order to facilitate the theoretical analysis in mathematics. Substituting Eq.(20) into Eqs.(13)–(19), we obtain the following dimensionless governing equations:

$$\frac{\partial^2\phi}{\partial r^2} + \frac{1}{r}\frac{\partial\phi}{\partial r} + \frac{1}{r^2}\frac{\partial^2\phi}{\partial\theta^2} + \frac{\partial^2\phi}{\partial z^2} = 0,$$

$$-h/R \le z \le \eta(r,\theta,t), \quad 0 < r < 1; \tag{21}$$

the boundary conditions at free surface $z{=}\eta$ $(r,\ \theta,\ t)$

$$\frac{\partial\eta}{\partial t} - \frac{\partial\phi}{\partial z} = W, \quad z = \eta(r,\theta,t); \tag{22}$$

$$\begin{cases} \varepsilon^2\left(2\dfrac{\partial^2\phi}{\partial r\partial z} + \dfrac{\partial W}{\partial r}\right) + \varepsilon^2\dfrac{\partial U}{\partial z} = 0, \\ \varepsilon^2\left(\dfrac{2}{r}\dfrac{\partial^2\phi}{\partial\theta\partial z} + \dfrac{1}{r}\dfrac{\partial W}{\partial\theta}\right) + \varepsilon^2\dfrac{\partial V}{\partial z} = 0, \end{cases}$$

$$z = \eta(r,\theta,t); \tag{23}$$

$$\frac{\partial\phi}{\partial t} + (1+\varepsilon\cos 2\omega_0 t)\eta + 2\nu\varepsilon^2\left(\frac{\partial^2\phi}{\partial z^2} + \frac{\partial W}{\partial z}\right) = 0,$$

$$z = \eta(r,\theta,t); \tag{24}$$

and the boundary conditions for the side-wall and the bottom of the vessel are

$$\nabla\phi + \boldsymbol{U} = 0, \quad z = -h/R \ \text{ and } \ r = 1. \tag{25}$$

The boundary layer equations are

$$\frac{\partial\boldsymbol{U}}{\partial t} = \varepsilon^2\nu\nabla^2\boldsymbol{U}, \tag{26}$$

$$\nabla\cdot\boldsymbol{U} = 0, \tag{27}$$

where U and V are velocity components of the boundary layer in r, θ directions respectively.

Recalling that the order of viscosity ν is $O(\varepsilon^2)$, and the thickness δ of an oscillatory boundary layer has an order of $O\{(2\nu/\Omega)^{1/2}\}$, so the order of the boundary layer thickness is $O(\varepsilon)$. A boundary layer coordinate is introduced as shown in Fig.2.

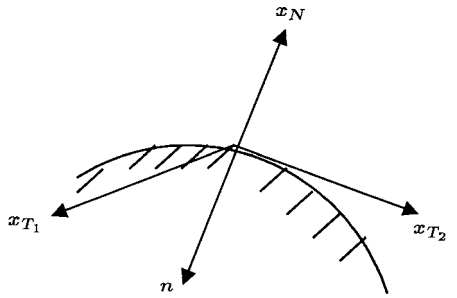

Fig.2. Curvilinear coordinates of the boundary layer.

Here x_N is the normal direction pointing into the fluid from the wall, hence opposite to $\boldsymbol{n}$. x_{T1} and x_{T2} determine the tangential plane that is perpendicular to the normal direction x_N. So x_N, x_{T1} and x_{T2} form a local rectangular coordinate system. We introduce a new boundary layer variable

$$\varsigma = \frac{x_N}{\varepsilon}. \tag{28}$$

Then the continuity equation (27) in terms of the local coordinate is

$$-\frac{\partial\boldsymbol{n}\cdot\boldsymbol{U}}{\partial\varsigma} + \varepsilon\left(\frac{\partial U_{T_1}}{\partial x_{T_1}} + \frac{\partial U_{T_2}}{\partial x_{T_2}}\right) = 0, \tag{29}$$

and the boundary layer equation (26) becomes

$$\frac{\partial\boldsymbol{U}}{\partial t} = \nu\frac{\partial^2\boldsymbol{U}}{\partial\varsigma^2}, \tag{30}$$

due to the supposition of weak viscosity.

In the next section, we will solve potential equation (21) with boundary condition (22)–(25) and boundary layer equations (29) and (30) by the method of perturbation expansions.

4. A series solution of external potential flow and inner boundary layer

We invoke two-time scale perturbation expansions, and expand the related variables into power series of the small parameter ε. A slowly varying time scale τ is introduced, such that

$$\tau = t\varepsilon. \tag{31}$$

Expand velocity potential ϕ, free surface displacement η and velocity vector $\boldsymbol{U}$ of the boundary layer into

$$\begin{cases} \phi = \phi_0(r,\theta,z,t,\tau) + \varepsilon\phi_1(r,\theta,z,t,\tau) + \cdots \\ \eta = \eta_0(r,\theta,t,\tau) + \varepsilon\eta_1(r,\theta,t,\tau) + \cdots \\ \boldsymbol{U} = \boldsymbol{U}_0(r,\theta,z,t,\tau) + \varepsilon\boldsymbol{U}_1(r,\theta,z,t,\tau) + \cdots \end{cases} \tag{32}$$

and then expand Eqs.(22) and (24) into Taylor series about z =0. Provided that we neglect higher-order terms O (ε^2), substitute Eqs.(31), (32) into Eqs.(21)–(25), compare with the coefficients of the small parameter ε^i at the two hands of all equations, and obtain governing equations and boundary conditions for both potential flow and boundary layer in every order of the ε^i.

Due to the complexity of the mathematical formulation, the detailed process is ignored in this paper, and only the important results are given as follows.

The external O (ε^0) velocity potential ϕ_0 (r, θ, z, t, τ) and free surface displacement η_0 (r, θ, t, τ) can be expressed as

$$\begin{aligned}\phi_0 =&J_m(\lambda r)\cosh[\lambda(z+h/R)]\\ &\times[p(\tau)\mathrm{e}^{\mathrm{i}\Omega t}+\bar{p}(\tau)\mathrm{e}^{-\mathrm{i}\Omega t}]\cos m\theta,\end{aligned}\tag{33}$$

$$\begin{aligned}\eta_0 =&-\mathrm{i}\Omega J_m(\lambda r)\cosh\lambda\\ &\times[p(\tau)\mathrm{e}^{\mathrm{i}\Omega t}-\bar{p}(\tau)\mathrm{e}^{-\mathrm{i}\Omega t}]\cos m\theta,\end{aligned}\tag{34}$$

where $J_m(r)$ is the m-order Bessel function of the first kind; the wavenumber $\lambda=\lambda_{mn}$ satisfies

$$\mathrm{d}J_m(\lambda_{mn}r)/\mathrm{d}r|_{r=1}=0,\tag{35}$$

$p(\tau)$ is called the slowly varying complex amplitude, $\bar{p}(\tau)$ denotes the complex conjugate of $p(\tau)$, and Ω is the natural frequency of the surface wave. The dispersion relationship obeys

$$\Omega^2=\lambda_{mn}\tanh(\lambda_{mn}h/R)=\lambda\tanh(\lambda h/R).\tag{36}$$

The internal boundary layers in our vertically forcing model are composed of side-wall layer and bottom layer. Both of them have three velocity components.

First of all, let U_{0W}, V_{0W} and W_{0W} be the three velocity components of the side-wall boundary layer. We have the velocity U_{0W} =0 from Eq.(25) and the boundary condition of the O (ε^0) potential flow. The appropriate fast coordinate is introduced by

$$\varsigma_W=\frac{r-1}{\varepsilon}.\tag{37}$$

The solutions of V_{0W} and W_{0W} can be formulated as follows:

$$\begin{aligned}V_{0W} =&mJ_m(\lambda)\cosh\lambda(z+h/R)\sin m\theta\\ &\times\Big[p(\tau)\mathrm{e}^{\mathrm{i}\Omega t}\mathrm{e}^{-(1+\mathrm{i})\sqrt{\frac{\Omega}{2\nu}}\varsigma_W}\\ &+\bar{p}(\tau)\mathrm{e}^{-\mathrm{i}\Omega t}\mathrm{e}^{-(1-\mathrm{i})\sqrt{\frac{\Omega}{2\nu}}\varsigma_W}\Big],\end{aligned}\tag{38}$$

$$\begin{aligned}W_{0W} =&-\lambda J_m(\lambda)\sinh\lambda(z+h/R)\cos m\theta\\ &\times\Big[p(\tau)\mathrm{e}^{\mathrm{i}\Omega t}\mathrm{e}^{-(1+\mathrm{i})\sqrt{\frac{\Omega}{2\nu}}\varsigma_W}\\ &+\bar{p}(\tau)\mathrm{e}^{-\mathrm{i}\Omega t}\mathrm{e}^{-(1-\mathrm{i})\sqrt{\frac{\Omega}{2\nu}}\varsigma_W}\Big].\end{aligned}\tag{39}$$

In the same way, by introducing an appropriate fast coordinate

$$\varsigma_B=\frac{z+h/R}{\varepsilon},\tag{40}$$

the solutions for bottom boundary layer U_{0B} and V_{0B} (similarly W_{0B}=0) can be described as

$$\begin{aligned}U_{0B} =&-\left(\frac{m}{r}J_m(\lambda r)-\lambda J_{m+1}(\lambda r)\right)\cos m\theta\\ &\times\Big[p(\tau)\mathrm{e}^{\mathrm{i}\Omega t}\mathrm{e}^{-(1+i)\sqrt{\frac{\Omega}{2\nu}}\varsigma_B}\\ &+\bar{p}(\tau)\mathrm{e}^{-\mathrm{i}\Omega t}\mathrm{e}^{-(1-i)\sqrt{\frac{\Omega}{2\nu}}\varsigma_B}\Big],\end{aligned}\tag{41}$$

$$\begin{aligned}V_{0B} =&\frac{m}{r}J_m(\lambda r)\sin m\theta\\ &\times\Big[p(\tau)\mathrm{e}^{\mathrm{i}\Omega t}\mathrm{e}^{-(1+i)\sqrt{\frac{\Omega}{2\nu}}\varsigma_B}\\ &+\bar{p}(\tau)\mathrm{e}^{-\mathrm{i}\Omega t}\mathrm{e}^{-(1-i)\sqrt{\frac{\Omega}{2\nu}}\varsigma_B}\Big].\end{aligned}\tag{42}$$

At O (ε^1), an inhomogeneous problem for ϕ_1 is obtained. In fact, we need not solve this inhomogeneous equation accurately, and can obtain the damping coefficient by virtue of the so-called solvability condition. The derived amplitude equation is

$$\frac{\mathrm{d}p(\tau)}{\mathrm{d}\tau}=-\mathrm{i}\alpha\bar{p}(\tau)+\beta p(\tau),\tag{43}$$

where α is a positive real number which represents the effect of vertical external excitation, and β denotes the complex damping coefficient. The detailed expressions of α and β are

$$\alpha=\frac{\Omega}{4},\quad \beta=\beta_W+\beta_B+\beta_M,\tag{44}$$

where β_W, β_B, and β_M represent the viscous damping on the side-wall, in the bottom boundary layer, and the meniscus region (this region is defined as the overlap between free surface and the side-wall boundary layer) respectively, and they can be written as

$$\beta_W=\frac{\lambda[\sinh(2\lambda h/R)+2\lambda h/R]}{8\Omega\cosh^2(\lambda h/R)}\sqrt{\frac{2\nu}{\Omega}}(1+\mathrm{i}),\tag{45}$$

$$\beta_B=\frac{\lambda^2}{4\Omega\cosh^2(\lambda h/R)}\sqrt{\frac{2\nu}{\Omega}}(1+\mathrm{i}),\tag{46}$$

$$\beta_M=\frac{\lambda^2\Omega}{2(\lambda^2-m^2)}\sqrt{\frac{2\nu}{\Omega}}(1+\mathrm{i}).\tag{47}$$

Henderson[20] pointed out that the real and the imaginary parts of Eqs.(45)–(47) mean the value of damping and frequency shift respectively. Damping causes the attenuation of the surface wave, while the frequency shift changes the natural frequency of the surface wave.

5. The critical condition for the appearance of stable surface waves

Separating Eq.(43) into real and imaginary parts, and letting

$$p(\tau) = p_1(\tau) + \mathrm{i}p_2(\tau), \quad \beta = \beta_1 + \mathrm{i}\beta_2, \tag{48}$$

we can express Eq.(43) as

$$\frac{\mathrm{d}p_1(\tau)}{\mathrm{d}\tau} = \beta_1 p_1(\tau) - (\alpha + \beta_2)p_2(\tau), \tag{49}$$

$$\frac{\mathrm{d}p_2(\tau)}{\mathrm{d}\tau} = -(\alpha - \beta_2)p_1(\tau) + \beta_1 p_2(\tau). \tag{50}$$

The ordinary differential equation groups (49) and (50) are linear and their instability condition can be easily obtained as

$$\alpha^2 > |\beta|^2. \tag{51}$$

Equation (51) means that the vertical external excitation cannot be smaller than the damping of the fluid if the surface wave is to be excited, and $|\beta|^2 = \beta_1^2 + \beta_2^2$.

Substituting Eqs.(44)–(47) into Eq.(51), and using the dispersive relation (36), we have

$$[(\lambda \tanh(\lambda h/R))]^{1/4} > \sqrt{\nu} \times \left(\frac{4\lambda^2}{(\lambda^2 - m^2)} + \frac{\sinh(2\lambda h/R) + 2\lambda h/R + 2\lambda}{\sinh(\lambda h/R)\cosh(\lambda h/R)}\right). \tag{52}$$

In order to make clear the physical meaning of the damping coefficient, the dimensional forms of Eqs.(44)–(47) and (52) become

$$\alpha = \frac{\Omega}{4}\sqrt{\frac{R}{g}},$$

$$\beta_W = \frac{g\sqrt{g/R}\lambda(\sinh 2\lambda h + 2\lambda h)}{32A\Omega^3\cosh^2(\lambda h)}\sqrt{\frac{2\nu}{\Omega}}(1+\mathrm{i}),$$

$$\beta_B = \frac{g\sqrt{gR}\lambda^2}{16A\Omega^3\cosh^2(\lambda h)}\sqrt{\frac{2\nu}{\Omega}}(1+\mathrm{i}),$$

$$\beta_M = \frac{R\sqrt{gR}\lambda^2}{8A\Omega(\lambda^2R^2 - m^2)}\sqrt{\frac{2\nu}{\Omega}}(1+\mathrm{i}),$$

$$A > \left[\frac{\sinh 2\lambda h + 2\lambda h + 2\lambda R}{4R\sinh\lambda h\cosh\lambda h} + \frac{\lambda^2 R}{(\lambda^2R^2 - m^2)}\right] \times \sqrt{\nu}/[g(\lambda\tanh\lambda h)^5]^{1/4}. \tag{53}$$

In Eq.(53), the expression of ε in Eq.(20) is employed.

6. Properties of the damping coefficient obtained by computation

6.1. Variation of the damping coefficient with viscosity and depth of the fluid

Figure 3 illustrates the damping coefficient as a function of viscosity.

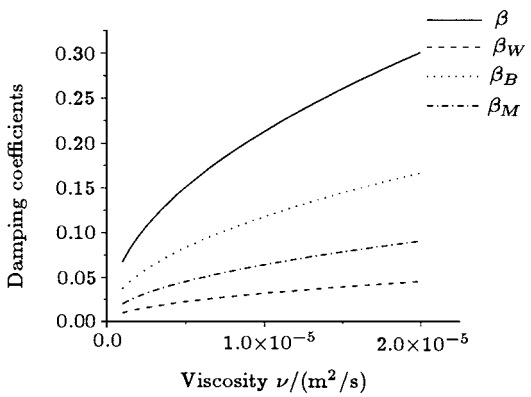

Fig.3. Variation of damping coefficient with viscosity (forced amplitude A=11.4μm, forced frequency f=8.5Hz,radius of the vessel R=7.5cm, depth of the fluid h=1.0cm).

It can be shown from Fig.3 that the damping coefficient of the side-wall, the bottom and the meniscus regions increase with the increase of viscosity. This obvious result can be easily seen from Eq.(53).

Figure 4 shows the variations of damping coefficient at different depth of the liquid layer.

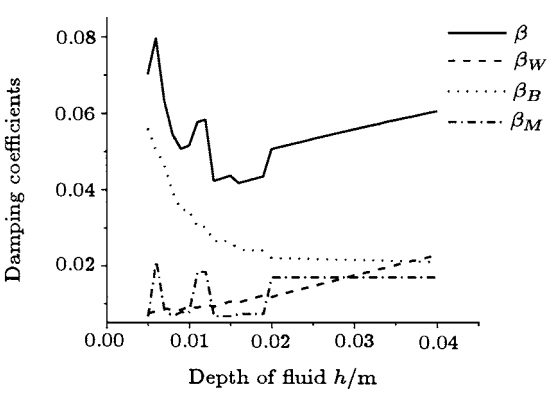

Fig.4. Variation of damping coefficient with the depth of fluid (forced amplitude A=11.4μm, forced frequency f=9Hz, radius of the vessel R=7.5cm, viscosity coefficient ν=10^{-6}m^2/s).

With the increase in the depth of the liquid, the area of the side-wall boundary layer increases accordingly, so the damping on the side-wall will increase too.

However, the damping of the bottom decreases with the increase in the depth of the fluid. As the fluid layer becomes shallow, the whole damping is primarily concentrated on the bottom boundary layer. In the region of the meniscus, the damping exhibits a jump in a certain depth. This is mainly due to the variability of mode selection, which can change the value of denominator in Eq.(53). When the depth of the fluid layer exceeds 2.0cm, the damping in the meniscus region increases with increasing depth of the fluid.

6.2. Variation of the damping coefficient with the forced amplitude and frequency

The dependence of the damping coefficient upon the forced amplitude is shown in Fig.5.

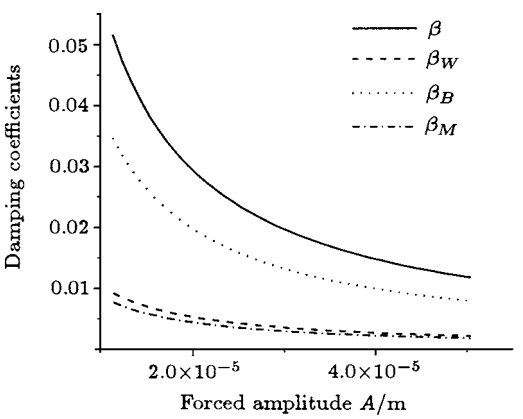

Fig.5. Variation of damping coefficient with forced amplitude (forced frequency f=9Hz, radius of the vessel R=7.5cm, depth of fluid h=1.0cm, viscosity coefficient ν=10^{-6}m^2/s).

Clearly, the damping decreases with the increase of the forced amplitude. The reason is that the energy entering into the system by external excitation is more than that of dissipation caused by viscosity. Under this condition, the energy will be accumulated and the surface wave becomes unstable. In fact, since the forced frequency is fixed, the small parameter ε will become larger with the increase of the forced amplitude and thus the basis of the theoretical analysis will not be satisfied.

Figure 6 illustrates the variation of damping coefficient with forced frequency.

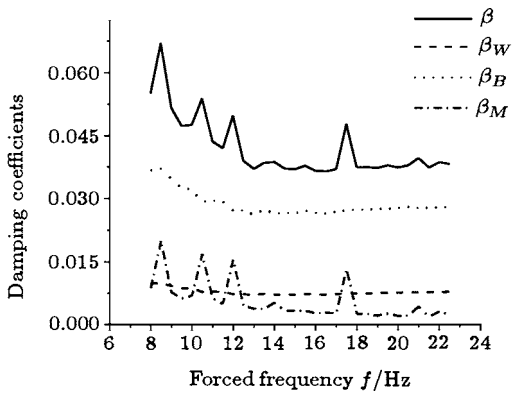

Fig.6. Variation of damping coefficient with forced frequency (forced amplitude A=11.4μm, radius of the vessel R=7.5cm, depth of fluid h=1.0cm, viscosity coefficient ν=10^{-6}m^2/s).

As indicated in the figure, the damping decreases gradually with the increase of forced frequency. The reasons are similar as for Fig.5. The damping of the meniscus is influenced by the selected mode of the surface wave as in Fig.4, while some jump phenomena appear.

6.3. Variation of damping coefficient with the radius of the vessel

The variation of damping coefficient with the radius of the vessel is shown in Fig.7, in which damping increases with the radius of the vessel.

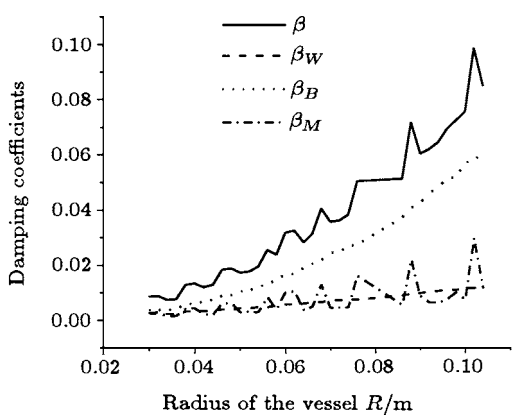

Fig.7. Variation of damping coefficient with the radius of vessel (forced amplitude A=11.4μm, forced frequency f=12Hz, depth of fluid h=1.0cm, viscosity coefficient ν=10^{-6}m^2/s).

A reasonable explanation is that the contact area between side-wall and fluid is enlarged. Thus the area of the boundary layer increases, and viscous damping increases accordingly.

6.4. Determination of the critical curve

When the forced amplitude and forced frequency exceed some threshold values, the system becomes un-

stable and surface waves form. From Eq.(53), we obtain a critical curve of forced amplitude versus forced frequency in Fig.8 by considering the dispersive relation (36).

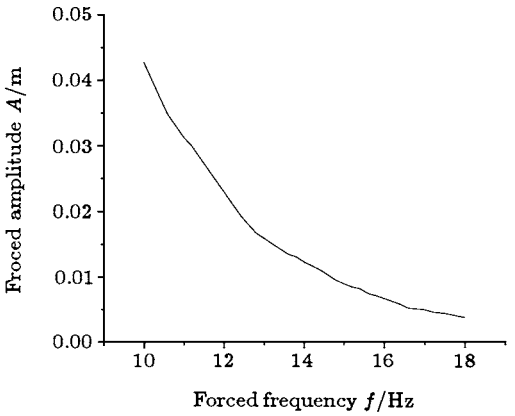

Fig.8. Critical curve associated with excited amplitude and forced frequency (depth of fluid h=1.0cm, radius of the vessel R=7.5cm, viscosity coefficient ν=10^{-6}m^2/s).

It is shown in Fig.8 that this curve approximates a hyperbola, and when the exciting frequency is small, the exciting amplitude must be large enough to produce a surface wave, and vice versa. It should be pointed out that the unstable region is the area above the curve.

6.5. The influence of viscous damping and surface tension on mode selection and comparison with experiment

In this section, we investigate the effect of the viscous damping in Eq.(53) on the natural frequency of the surface wave and mode choice. The natural frequency (36) was modified by introducing the imaginary part of the viscous damping coefficient β_2, which is the sum of dampings of side-wall, bottom and meniscus in Eq.(53),

$$\hat{\Omega} = \Omega - \beta_2, \tag{54}$$

where

$$\begin{aligned}\Omega &= \sqrt{\lambda \tanh(\lambda h/R)},\\ \beta_2 &= \left[\frac{\lambda[\sinh(2\lambda h/R)+2\lambda h/R]}{8\Omega\cosh^2(\lambda h/R)}\right.\\ &\quad \left.+\frac{\lambda^2}{4\Omega\cosh^2(\lambda h/R)}+\frac{\lambda^2\Omega}{2(\lambda^2-m^2)}\right]\sqrt{\frac{2\nu}{\Omega}}.\end{aligned} \tag{55}$$

In order to show the influence of surface tension and damping on the pattern selection, we present a frequency versus wavenumber curve in Fig.9.

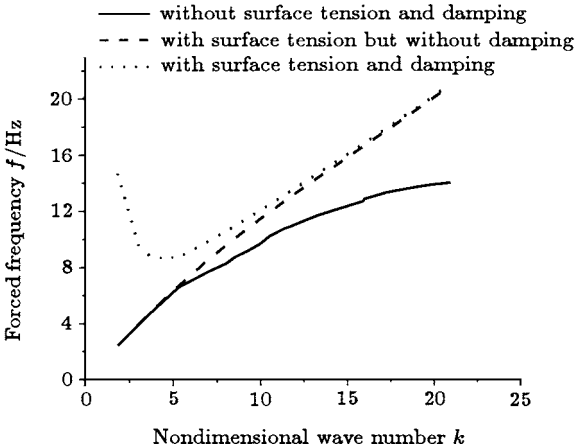

Fig.9. Variation of dimensional natural frequency and modified frequency with wavenumber (depth of fluid h=1.0cm, radius of the vessel R=7.5cm, viscosity coefficient ν=10^{-6}m^2/s).

It can be seen from Fig.9 that when the forcing frequency is low, the viscosity of the fluid is a prominent factor for the mode selection. However, when the forcing frequency is high, the surface tension of the fluid is the prominent.

Table 1 and Fig.10 illustrate the comparison of the forced frequencies in theory for different patterns including the effect of surface tension and damping with those in experiment. In Fig.10, the left figures show the calculated results (the meanings of parametrical couple (m, n), solid lines and dashed lines are the same as in Refs.[16, 17]), and the right ones are the experimental contours of flow patterns.

It is found from Table 1 and Fig.10 that when the wavenumber is low, e.g. (3, 3) mode, the forced frequency agrees well with the experimental result. However, when the wavenumber is high, the forced frequency is quite different from the experimental result. This is possibly due to the dissipation of the moving contact line of the meniscus, the mode competition in high frequency, and the surface viscosity of surfactant films, which are ignored in our present analysis.

7. Conclusions

From the above analysis, the following results can be obtained:

1. The analytical expression of the damping coefficient is obtained and its properties have been studied over a range of system parameters. Viscous damping increases with viscosity, depth of fluid and radius of the vessel, and decreases with the external amplitude or frequency of excitation.

2. An instable condition for the occurrence of surface waves is determined and the critical curve is obtained analytically.

3. When the wavenumber is small, the influence of the damping is important. However, when the wavenumber is large, the effect of surface tension is prominent.

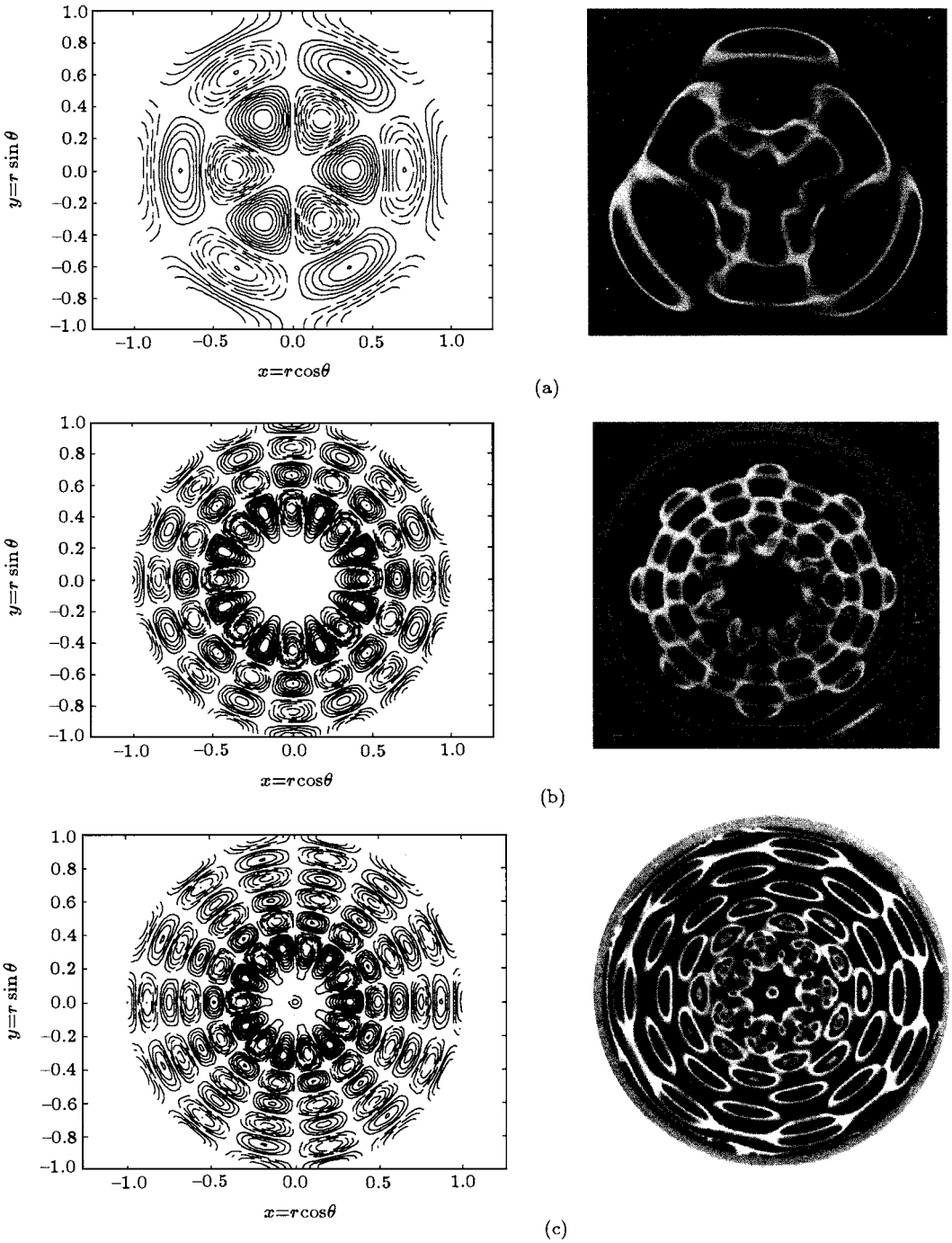

Fig.10. Comparison of theoretical contours of surface wave mode with those of experiment (depth of fluid h=1.0cm, radius of the vessel R=7.5cm, the forcing amplitude A=11.4μm). (a) (3, 3) mode (left) forced frequency f=19.9, (right) forced frequency f=20Hz, (b) (8, 4) mode (left) forced frequency f=22.5Hz, (right) forced frequency f=50Hz, (c) (7, 6) mode (left) forced frequency f=26.7 Hz, (right) forced frequency f=52Hz.

Table 1. Comparison of the forced frequencies in theory for different patterns including the effect of surface tension and damping with those in experiment.

Pattern (m, n)	Wave number	Forced frequency without surface tension and damping/Hz	Forced frequency with surface tension and without damping/Hz	Forced frequency with surface tension and damping/Hz	Experimental forced frequency/Hz
(3, 3)	11.346	11.68	12.63	19.9	20
(8, 4)	21.229	16.71	21.10	22.5	50
(7, 6)	26.545	18.74	26.02	26.7	52

Acknowledgement

The authors are grateful to Professor Zhou Xianchu for discussion on the aspects of mathematical treatment, and Dr Bai Wei for assistance with the numerical work.

References

[1] Faraday M 1831 *Philos. Trans. R. Soc. London* **121** 319
[2] Benjamin T B and Ursell F 1954 *Proc. R Soc. London* **255** 505
[3] Miles J W 1976 *J. Fluid Mech.* **75** 419
[4] Miles J W 1984 *J. Fluid Mech.* **148** 451
[5] Miles J W 1993 *J. Fluid Mech.* **248** 671
[6] Miles J W and Henderson D 1990 *Ann. Rev. Fluid Mech.* **22** 143
[7] Edwards W S and Fauve S 1994 *J. Fluid Mech.* **278** 123
[8] Müller H W 1993 *Phys. Rev. Lett.* **71** 3287
[9] Kumar K and Bajaj K 1994 *Phys. Rev.* E **52** R4606
[10] Ezerskii A B*et al* 1985 *Zh. Eksp. Theor. Fiz.* **41** 129 (transl. 1986 *Sov. Phys. JEPT Lett.* **41** 157)
[11] Tufillaro N *et al* 1989 *Phys. Rev. Lett.* **62** 442
[12] Ciliberto S *et al* 1991 *Europhys. Lett.* **15** 23
[13] E X Q and Gao Y X 1996 *Commun. Nonlinear Sci. Numer. Simul.* **1** 1
[14] E X Q and Gao Y X 1996 *Proc. 4th Asian Symp. on Visualization Beijing* 653
[15] Gao Y X and E X Q 1998*Exp. Mech.* **13** 326 (in Chinese)
[16] Jian Y J *et al* 2003 *Appl. Math. Mech.* **24** 1194 (English edition)
[17] Jian Y J and E X Q 2003 *J. Hydrodynam.* **18** 135 (in Chinese)
[18] Jian Y J 2003 *PhD Thesis* Institute of Mechanics, Chinese Academy of Sciences
[19] Hill D F 2002 *Phys. Fluids* **14** 158
[20] Henderson D M 1998 *J. Fluid Mech.* **365** 89